

## Chapter 2

# Signal Acquisition and Preprocessing

**Abstract** This chapter describes the detailed settings of the knee joint vibroarthrographic signal acquisition system. The text also presents a cascade moving average filter method to estimate the baseline wander in the raw signal, along with the combination of the ensemble empirical mode decomposition and detrended fluctuation analysis algorithms to remove the random noise. The filtering techniques for reduction of muscle contraction interference are also reviewed in the chapter.

### 2.1 Signal Analysis Procedures

The common flowchart of VAG signal analysis procedures is shown in Fig. 2.1. The data acquisition system collects the raw time series and conditions the signal with bandpass filters and amplifiers. The task of the signal preprocessing procedure is to remove the artifacts in the raw signal. Such artifacts mainly include baseline wander, random noise, and periodical power-line interference. With the artifact-free signal, several computational methods can then be employed to study the signal in the time scale or time-frequency domain. Advanced approaches can also be applied to characterize the fractal and statistical properties of the VAG signal. The distinct features extracted from the signal provide the particular information about the signal variability and complexity in waveform shifting, frequency range, or statistics [16–18]. The feature computing procedure mainly focuses on combining and refining the most informative feature sets, by using feature selection or mapping techniques [20]. Finally, the pattern analysis tools can be utilized to distinguish the pathological signals recorded from symptomatic patients and the normal signals recorded from healthy subjects [3, 28, 34].

### 2.2 Signal Acquisition

As shown in Fig. 2.2, VAG signals can be recorded with one or more accelerometers [9, 21, 22] or an electro-stethoscope [8]. The sensor can be taped to the subject's patella [21, 22, 24], middle of the patella [9, 24, 38], lateral condyle of the tibia

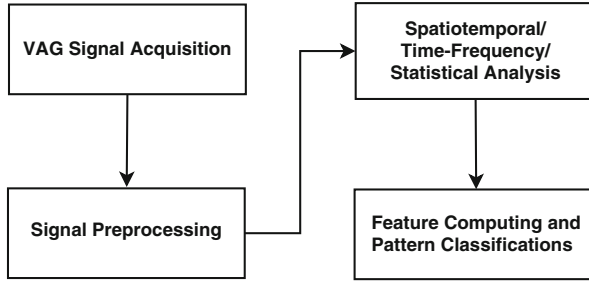


**Fig. 2.1** Diagram of knee joint VAG signal analysis methodology

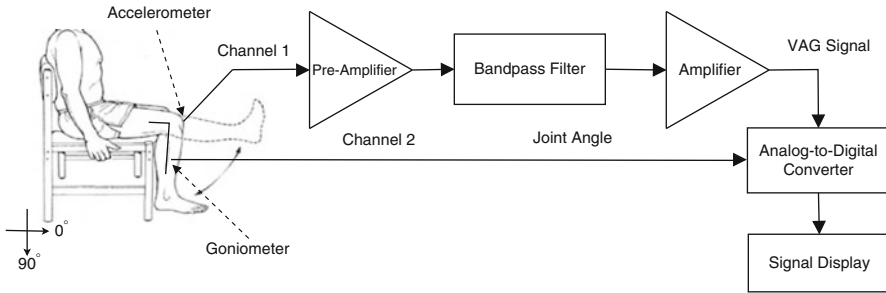


**Fig. 2.2** Knee joint vibroarthrographic (VAG) data acquisition setup. Channel 1 records the VAG signal at the middle position of patella; channel 2 records goniometer voltage (angle) information

[24, 25, 38], medial condyle of the tibia [8, 24], or tibial tuberosity [24, 38], by using two-sided adhesive tapes. The subjects are commonly asked to bend the leg at the knee joint (reducing the angle between the shank and thigh), and straighten the leg until the full knee extension. The accelerometer sensor can measure the acceleration and deceleration amplitude of the knee joint in the course of flexion or extension. In addition to the accelerometer or stethoscope sensor, a VAG signal acquisition system may also consist of an electro-goniometer in order to measure the bending angle of the leg during the knee flexion or extension. Before the signal recording, it is necessary to appropriately configure the supporting devices and software, which commonly contain anti-aliasing bandpass filters, amplifiers, analog-to-digital converter, graphic signal display, and signal condition toolkits.

This book presents the VAG signal acquisition system and the experimental protocol developed by the research group of Rangayyan [10, 12, 19, 24, 36], as a paradigm. A miniature accelerometer (Model 3115A, Dytran Instruments, Inc., Chatsworth, CA, USA) was adhered to the middle of the patella. The subjects were requested to sit on a rigid chair with the legs both freely suspended in air. During the signal recording procedure, each subject should voluntarily swing the shank tested over an angle range from  $135^\circ$  to  $0^\circ$  (extension movement), and back to  $135^\circ$  (flexion movement) in the duration of 4 s [19] (associated with an approximate angular velocity of  $67^\circ$  per second).

The raw time series was collected by an instrumentation recorder (Model 3968A, Hewlett Packard, San Diego, CA, USA) with a sampling rate of 2 kHz. Then, the acceleration signal was conditioned by a bandpass filter with a bandwidth of 10 Hz–1 kHz to prevent aliasing effects, and amplified by isolation pre-amplifiers (Model 11-5407-58, Gould Instrument Systems, Inc., Cleveland, OH, USA) and universal amplifiers (Model 13-4615-18, Gould Instrument Systems, Inc., Cleveland, OH, USA). The signal was digitized with a resolution of 12 bit per sample by using a data acquisition board (AT-MIO-16L, National Instruments, Austin, TX, USA) and the LabVIEW software (National Instruments, Austin, TX, USA).

Auscultation of the knee joint using a stethoscope was also performed to provide a qualitative description of sound intensity, along with the corresponding relationship to the angle of knee joint. For the subjects who underwent arthroscopic surgery, the lesion locations observed were used to estimate the joint angles at which the appeared articular surfaces would come into contact and affect the corresponding VAG signal segments.

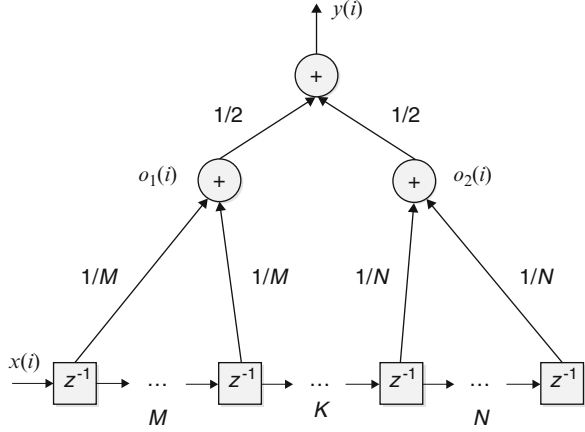
## 2.3 Signal Preprocessing

In clinical application, it is essential to record high-quality VAG signals for computer-aided diagnostic analysis of knee joint pathology [32]. However, recording of the knee joint VAG signals with the sensor on the contact surface of the subject's patella is susceptible to several different types of artifacts, including electromyogram, random noise, ambient interference, and baseline wander [2, 33]. The artifact of electromyogram is commonly induced by concurrent muscular contractions during the knee flexion or extension motion. Random noise due to the thermal effect in the ambient cables and amplifiers is inevitable in the signal acquisition procedure. Since the mechanism of random noise is complex and random, the range of signal-to-noise ratio of VAG signals cannot be determined a priori [32]. The major environmental interference is caused by 50 or 60 Hz power-supply lines and radio-frequency emissions from medical devices. However, the signal acquisition system driven by direct-current battery power supply is free of the periodical power-line interference. Sometimes, patients with knee joint disorders may tremble the legs due to skin friction or the painful reaction when they bending the leg in a vibration arthrometry examination, which would cause the baseline wander in the raw signal.

### 2.3.1 Removal of Baseline Wander

In order to remove the baseline wander in the VAG record, we may use a cascade moving average filter to estimate the such a artifact and then subtract it from the raw signal [2]. The moving average filter is a type of finite impulse response (FIR) filter

**Fig. 2.3** The hierarchical structure of the cascade moving average filter



that is frequently used for time series analysis. In the filtering procedure, temporal statistics are computed using a few samples of the signal along the time axis, and the samples in a temporal moving window are averaged to produce the output at various points of time [15]. Different from the conventional design of a moving average filter, the cascade moving average filter consists of a hierarchical structure that combines two-layer moving average operators, as shown in Fig. 2.3. The first layer of the cascade filter includes a  $M$ -order and a  $N$ -order successive moving average operators. The  $K$  inputs in the tail end of the  $M$ -order operator overlap with the beginning inputs of the  $N$ -order operator. The output of the  $M$ -order operator  $o_1(i)$  is written as

$$\begin{aligned} o_1(i) &= \frac{1}{M} [x(i-1) + \cdots + x(i-M)] \\ &= \frac{1}{M} \sum_{m=1}^M x(i-m), \end{aligned} \quad (2.1)$$

and the output of the following  $N$ -order operator  $o_2(i)$  can be expressed as

$$\begin{aligned} o_2(i) &= \frac{1}{N} [x(i-M+K) + \cdots + x(i-M+K-N)] \\ &= \frac{1}{N} \sum_{n=1}^N x(i-M+K-n). \end{aligned} \quad (2.2)$$

The second layer of the moving average filter is designed to smooth the piecewise linear trends obtained from the outputs of two moving average operators in the first layer. The final output of the cascade moving average filter is given by

$$\begin{aligned}
y(i) &= [o_1(i) + o_2(i)] / 2 \\
&= \frac{1}{2M} \sum_{m=1}^M x(i-m) + \frac{1}{2N} \sum_{n=1}^N x(i-M+K-n). \quad (2.3)
\end{aligned}$$

By applying the  $z$ -transform, we may compute the transfer function  $H(z)$  of the cascade moving average filter as

$$H(z) = \frac{Y(z)}{X(z)} = \frac{1}{2M} (z^{-1} + \dots + z^{-M}) + \frac{1}{2N} (z^{-M+K-1} + \dots + z^{-M+K-N}), \quad (2.4)$$

where  $X(z)$  and  $Y(z)$  are the  $z$ -transform of the filter input  $x(i)$  and output  $y(i)$ , respectively.

To estimate the baseline wander in the VAG signal, the two moving average operators in the first layer of the hierarchical model can be configured with the equal orders, i.e.,  $M = 20$  and  $N = 20$ , respectively. The reason for such a filter design is due to the symmetry of the leg swinging angles ( $135^\circ \rightarrow 0^\circ \rightarrow 135^\circ$ ) in the signal acquisition experiment. The number of the overlapping inputs of the moving average operators is set to be  $K = 5$ . The frequency response of the cascade moving average filter is shown in Fig. 2.4.

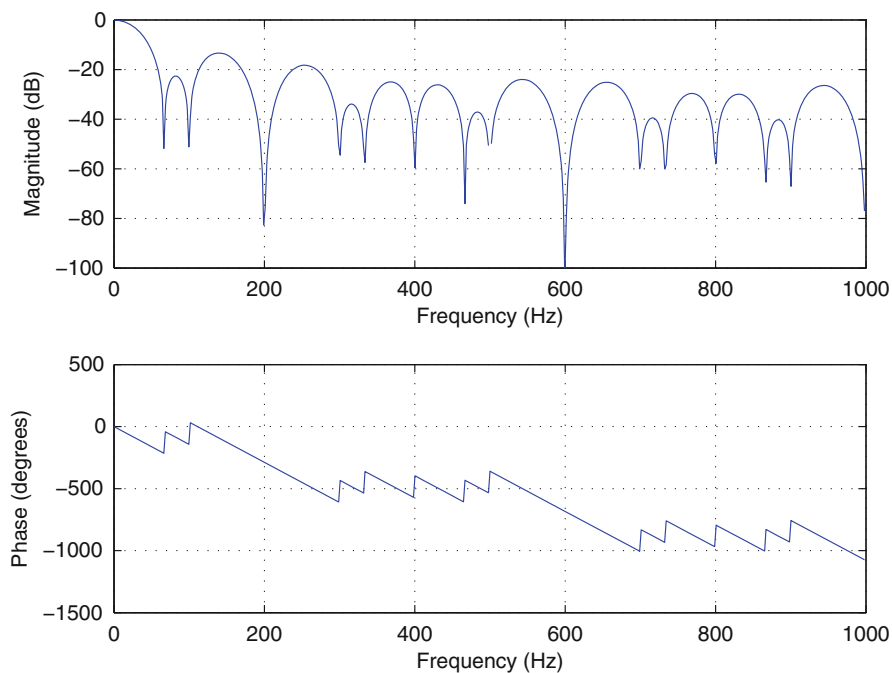


**Fig. 2.4** The frequency response of the cascade moving average filter for detrending the baseline wander in knee joint vibroarthrographic signal

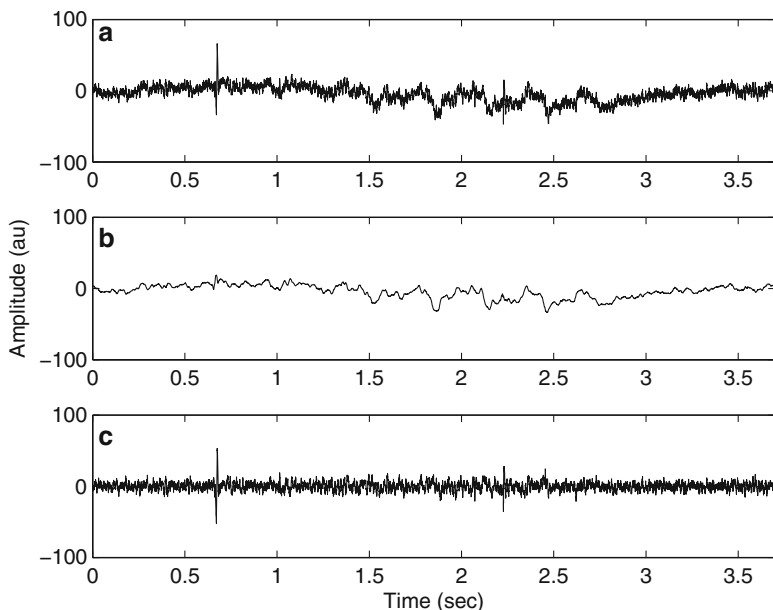


**Fig. 2.5** Subfigures from top to bottom: (a) the raw knee joint vibroarthrographic signal recorded from a healthy subject, (b) the baseline wander estimated by the cascade moving average filter, and (c) the baseline-wander-free signal of the filter output

The results of baseline wander removal in the VAG signals for a healthy subject and a patient (33-year-old male) with Grade II-III chondromalacia patellae are plotted in Figs. 2.5 and 2.6, respectively. It is noted that the normal VAG signal in Fig. 2.5a is contaminated with a few random noise, but the signal variation is relatively small in amplitude. The abnormal VAG signal in Fig. 2.6a dramatically fluctuates from 0.8 to 1.25 s, and later from 1.8 to 2.3 s, which corresponds to the pathological joint surface at the angle range from  $30^\circ$  to  $110^\circ$ . It can be observed from Fig. 2.5b that the baseline wander in the normal signal exhibits higher degree of regularity in the waveform than that in the pathological signal shown in Fig. 2.6b. The baseline wander estimated in Fig. 2.6b is caused due to the uncomfortable trembling of the leg in the course of knee extension and flexion through the degenerative joint surface. It is noted from Figs. 2.5c and 2.6c that the drifts have been effectively eliminated by the cascade moving average filter, and the baselines of the filtered VAG signals are placed back to the isoelectric line (the zero level).

### 2.3.2 Removal of Random Noise

The noise in the form of random fluctuations around the isoelectric line is a common type of artifacts in biomedical signals [11, 29, 31, 33]. The random noise could

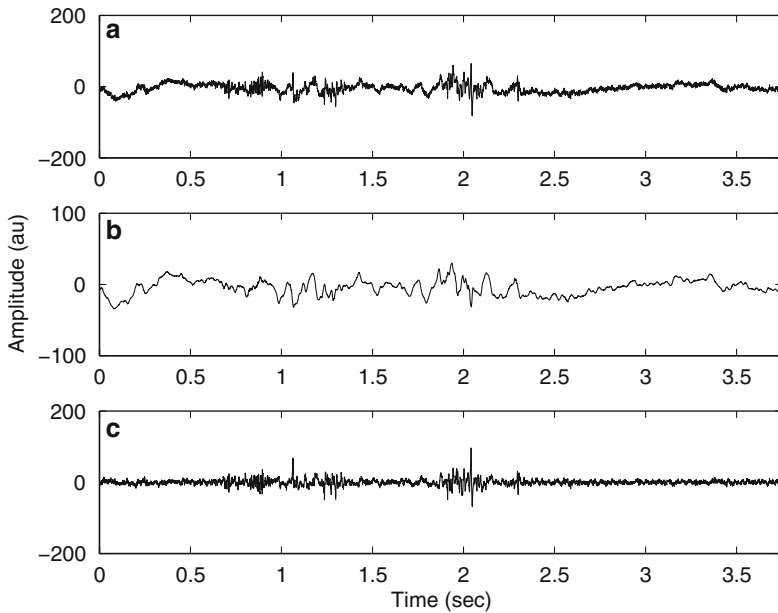


**Fig. 2.6** Subfigures from top to bottom: (a) the raw knee joint vibroarthrographic signal recorded from a patient (male, age: 33 years old) with Grade II-III chondromalacia patellae, (b) the baseline wander estimated by the cascade moving average filter, and (c) the baseline-wander-free signal output by the cascade moving average filter

be generated due to the unavoidable thermal effect or semiconductor defects of medical instruments [30]. In this section, we introduce an effective method that combines the ensemble empirical mode decomposition and detrended fluctuation analysis algorithms to remove random noise in the VAG signal [35]. The EEMD first divides the raw VAG signal into several intrinsic mode functions (IMFs) in the successive decomposition processes. The DFA algorithm is then applied to identify the inherent correlation property of each IMF. Finally, the IMFs that contain the dominant artifacts of random noise and monotonic baseline residue can be removed in the reconstructed artifact-reduced signal.

### 2.3.2.1 Ensemble Empirical Mode Decomposition

The empirical mode decomposition (EMD) was introduced by Huang et al. [4] as a popular technique for nonlinear and nonstationary signal analysis. The EMD method works by sifting a given signal into a set of intrinsic mode functions (IMFs) that represent the fast and slow oscillations in the signal [5]. Although this rationale shares much with the wavelet analysis philosophy, the IMFs with slow oscillations are not defined through any prescribed filtering operation [23]. For each IMF, the local maxima are all positive and the local minima are all negative [33].

The envelopes of the IMFs defined in the sifting operator are zero-crossing and symmetrical. For a signal that is composed of two or more spectral components, the EMD method has the capability to separate these components with different amplitude levels in the decomposed IMFs, as confirmed in the previous work of Rilling and Flandrin [23]. However, the effectiveness of the EMD method is limited by the mode mixing effect [6]. Mode mixing is a phenomenon that the oscillations with disparate time scales are preserved in one IMF, or that the oscillations with the same time scale are sifted into different IMFs.

Recently, Wu and Huang [27] proposed a noise-assisted EMD algorithm, called ensemble empirical mode decomposition (EEMD), to overcome the mode mixing obstacle. The EEMD adds different series of white noise into the signal in several trials [35]. The added white noise plays a crucial role in the decomposition process, because it provides uniformly distributed references of different scales [26]. In each trial, the added noise is different, such that the decomposed IMFs have no correlation with the corresponding IMFs from one trial to another. If the number of trials is sufficient, the added noise can be canceled out by ensemble averaging of the corresponding IMFs obtained in the different trials. The details of the EEMD process are described as follows [27].

1. In the  $n$ th trial, a white noise time series  $u_n(t)$  is added to a given signal  $x(t)$ , in order to attain a new time series  $y_n(t) = x(t) + u_n(t)$ ,  $n = 1, 2, \dots, N$ , where  $N$  denotes the number of ensemble.
2. The noise-contaminated signal  $y_n(t)$  is decomposed into a set of IMFs using the original EMD method [4], that is

$$y_n(t) = \sum_{j=1}^i c_j^n + r_i^n, \quad (2.5)$$

where  $i$  denotes the total number of the IMFs in each decomposition,  $c_j^n$  is the  $j$ th IMF, and  $r_i^n$  represents the residue of  $y_n(t)$  in the  $n$ th trial. To ensure that the number of IMFs in each decomposition to be equal, we may assign a fixed siftings number of 10, so as to produce the IMF in each VAG signal decomposition process.

3. The above two steps are repeated for  $N$  trials, with different white noise series  $u_n(t)$  added in each trial.
4. The corresponding  $j$ th IMFs obtained in the total  $N$  trials are averaged, that is

$$c_j^{ave} = \frac{1}{N} \sum_{n=1}^N c_j^n, \quad (2.6)$$

where  $c_j^{ave}$  is the final IMF of the EEMD.

The effectiveness of the EEMD method depends on the appropriate setting of the ensemble number and the amplitude of added white noise. Wu and Huang [27]



suggested that the number of ensemble ( $N$ ) and the amplitude of added noise ( $A$ ) should satisfy the following rule:

$$\varepsilon = \frac{A}{\sqrt{N}}, \quad (2.7)$$

where  $\varepsilon$  represents the final standard deviation of error, which indicates the difference between the original data and the sum of the IMFs produced by the EEMD method. The ratio of the standard deviation of the added noise and that of the raw VAG signal could be 0.2. And the number of ensemble could be fixed at  $N = 100$  to average the corresponding IMFs obtained in the total 100 trials of the EEMD.

Figure 2.7 shows the IMFs decomposed by the EEMD method from the VAG signal of a patient with anterior cruciate ligament (ACL) and chondromalacia in the knee. The EEMD provided the C1–C11 IMFs in the successive decomposition iterations, and remained the monotonic trend as the final residue. It is visualized in Fig. 2.7 that different IMFs exhibit the components of the raw signal with different levels of fluctuations. The first three IMFs (C1–C3) are composed of most of the fast (high-frequency) oscillations in the raw VAG signal. The IMFs decomposed at the higher levels (C4–C11), on the other hand, consist of more slow (low-frequency) oscillations. The distinct morphological characteristics associated with the pathological conditions of ACL (from 0.9 to 1.1 s and from 3.7 to 4 s) and chondromalacia (from 1.4 to 1.9 s) can be observed in the C4–C6 IMFs in Fig. 2.7.

### 2.3.2.2 Fractal Scaling Index

With the IMFs decomposed by the EEMD method, the next task is to identify whether an IMF contains the dominant artifacts in the knee joint VAG signal. In most cases, the artifacts and the signal components possess different correlation properties (for example, anti-correlated or long-range correlated). The detrended fluctuation analysis (DFA) algorithm can be applied to study such correlation properties of each IMF [35]. It is very popular for the detection of nonstationary time series that exhibit long-range correlation properties [1]. The DFA algorithm computes the fractal scaling index parameter that describes the subtle fluctuations associated with intrinsic correlations of the dynamics in the signal. The fractal scaling index ( $\alpha$ ) is often used to measure the statistical self-affinity of a signal [13, 14].

Given an  $L$ -length decomposed IMF  $c_j^{ave}(l)$  with the mean value of  $w_j$ , the integrated IMF time series  $s(m)$  is defined by

$$s(m) = \sum_{l=1}^m \left[ c_j^{ave}(l) - w_j \right]. \quad (2.8)$$

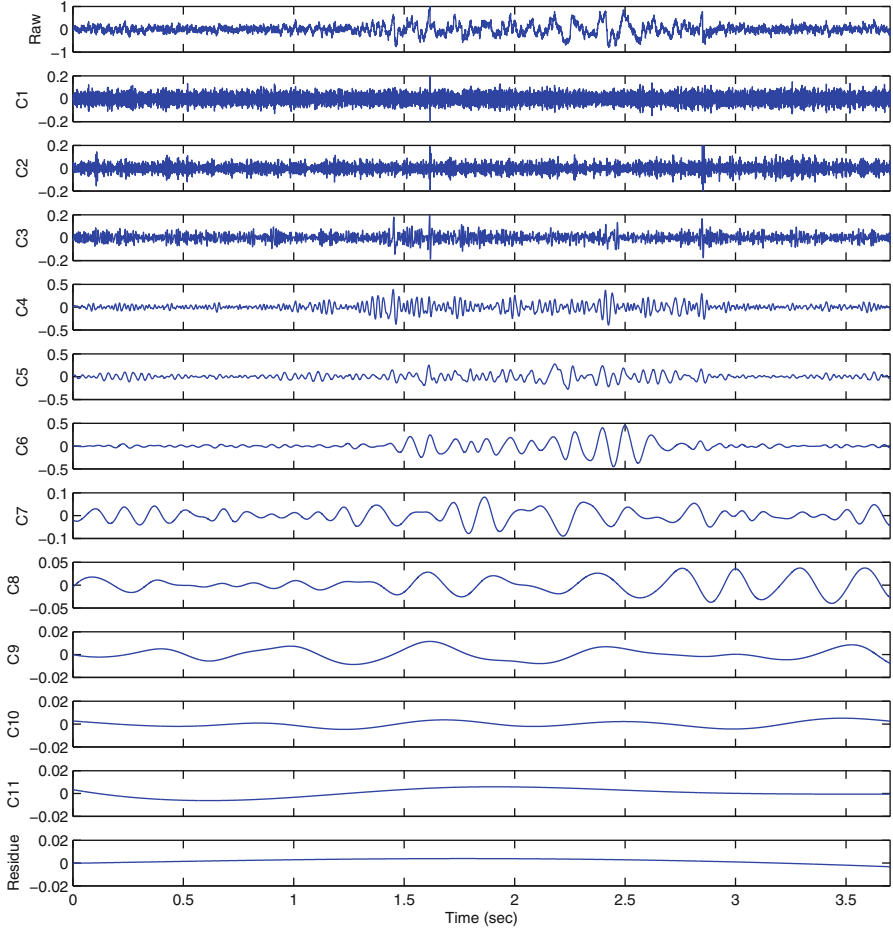


**Fig. 2.7** Plots of the intrinsic mode functions (IMFs) decomposed by the EEMD from the VAG signal of a patient with anterior cruciate ligament and chondromalacia. From top to bottom: the raw signal, the corresponding IMFs (C1–C11), and the monotonic trend (Residue)

The integrated time series  $s(m)$  is then divided into several window segments of equal size  $k$ , and a least-squares line (i.e., the local linear trend), denoted as  $s_k(m)$ , that fits the window samples. The local detrended fluctuation is then computed by subtracting the local linear trend  $s_k(m)$  from the integrated time series  $s(m)$  in each window segment. The averaged fluctuation  $F(k)$  is computed with the local detrended fluctuations in the root-mean-square sense as

$$F(k) = \left[ \frac{1}{L} \sum_{m=1}^L [s(m) - s_k(m)]^2 \right]^{\frac{1}{2}}. \quad (2.9)$$

For the VAG signal sampled at 2 kHz, the averaged fluctuation computation could be iteratively performed over the time scales defined by the window sizes in the range of from 10 to 250, with an increment of 20, for each decomposed IMF. The function relating the averaged fluctuation  $F(k)$  to the window size  $k$  is usually plotted with a double logarithmic graph. The fractal scaling index ( $\alpha$ ) is defined as the slope of the linear relationship between  $\log_{10} F(k)$  and  $\log_{10} k$ , which is expressed by a power law as  $F(k) \sim k^\alpha$  [14]. In the case of  $0.5 < \alpha < 1$ , the integrated and detrended time series possess persistent long-range power-law correlations, whereas  $0 < \alpha < 0.5$  indicates an anti-correlated property of the time series [7]. Typically, the fractal scaling index  $\alpha = 0.5$  indicates the integrated and detrended time series is considered as white noise [13]. For the pink noise ( $1/f$  noise) and Brown noise, the fractal scaling index values of the integrated and detrended time series are  $\alpha = 1$  and  $\alpha = 1.5$ , respectively [13].

To identify the artifact components in the VAG signal, the DFA algorithm is implemented to compute the fractal scaling index ( $\alpha$ ) value for each IMF. The double-logarithmic relationships between the averaged fluctuation and the window size for the C1, C6, and C8 IMFs are displayed in Fig. 2.8. It is clear that these three IMFs possess different  $\alpha$  values, i.e., the slope of the linear fitting in the root-mean-square sense. The fractal scaling index value of the C1 IMF is equal to 0.14, which

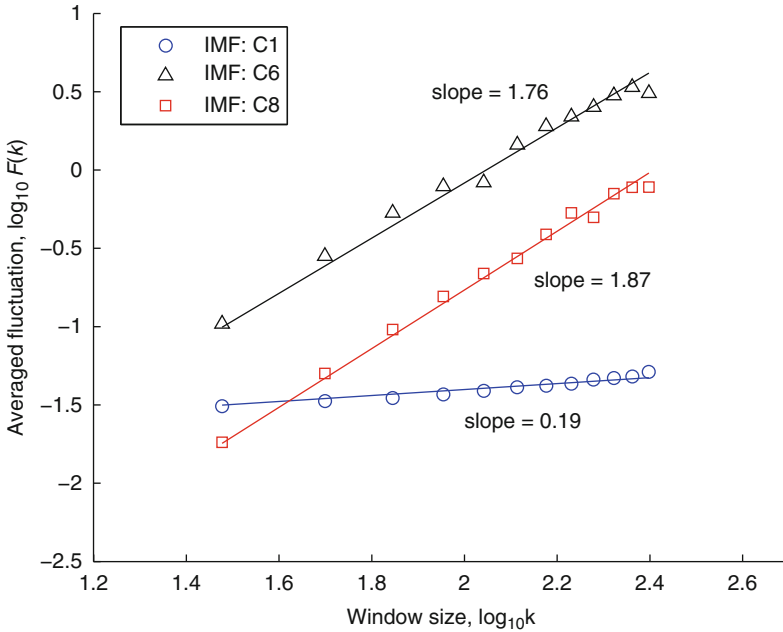


**Fig. 2.8** Double logarithmic plots of the linear relationship between averaged fluctuation  $F(k)$  and the window size  $k$ , for the IMFs C1, C6, and C8, decomposed from the VAG signal of a patient with anterior cruciate ligament and chondromalacia

indicates that such an IMF contains plenty of anti-correlated components. The  $\alpha$  values of the C6 and C8 IMFs are larger than 1.5, which implies that both of these IMFs are with long-range power-law correlations. The C6 IMF ( $\alpha = 1.6$ ) involves less long-range correlated components than the C8 IMF ( $\alpha = 1.86$ ), because the C6 IMFs contains more fast oscillations of the VAG signal. Since the random noise are not long-range correlated, the VAG signal can be reconstructed with the long-range correlated IMFs ( $\alpha > 0.5$ ), such that the IMFs with anti-correlations ( $0 < \alpha < 0.5$ ) and the final monotonic residue (baseline wander) are considered as artifacts. A comparison of the raw VAG signal and the reconstructed artifact-reduced signal is shown in Fig. 2.9. It is clear that the removed artifacts in Fig. 2.9b contains a larger number of fast oscillations, and the morphological segments associated with the pathological conditions are not distorted in the artifact-free VAG signal in Fig. 2.9c. It is also worth noting that there still exist some components with rapidly variations in the reconstructed VAG signal in Fig. 2.9c. These long-range correlated components are the mechanomyographic and vibromyographic responses of the superficial muscles contracted in the duration of knee flexion and extension in the signal acquisition procedure.

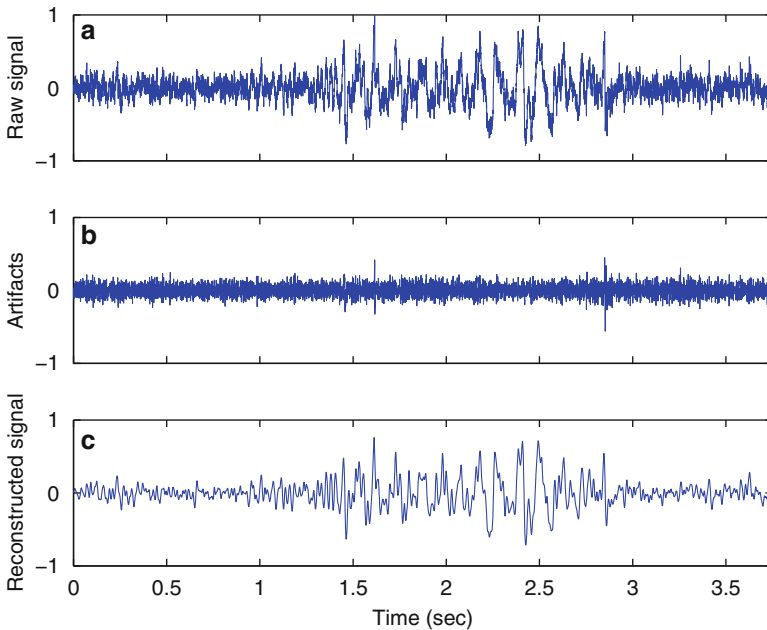


**Fig. 2.9** Subfigures from top to bottom: (a) the raw knee joint vibroarthrographic signal a patient with anterior cruciate ligament and chondromalacia, (b) the noise components decomposed by the ensemble empirical mode decomposition method, and (c) the reconstructed artifact-free signal

### 2.3.3 *Reduction of Muscle Contraction Interference*

Muscle contraction interference (MCI) is another type of dominant artifacts that may obscure the VAG signal analysis. MCI involves the effects of vibromyogram (VMG) associated with contraction of skeletal muscles [37, 39]. The VMG signal, also known as the muscle sound, is the acoustic manifestation of the mechanical activity of muscle fibers, and can be detected with accelerometers placed on the skin surface over an active muscle. Zhang et al. [37] compared simultaneous recordings of VMG and electromyogram (EMG) generated by skeletal muscles during voluntary isometric and isotonic contractions. Their results suggested that the VMG and EMG signals are equally sensitive to muscle contraction levels at various joint angles, and that the frequency and intensity of the VMG signal vary in direct proportion to the muscular contraction level. To reduce the MCI, Zhang et al. [39] applied a two-stage least-mean-squares (LMS) adaptive filter. The first stage was used to remove the measurement noise in the accelerometers and associated amplifiers, and the second stage was designed to cancel the muscle signal. The step size of the LMS adaptive filter was optimized by using a root-mean-squared-error-based gradient noise (or misadjustment) factor and a time-varying estimate of the input signal power [36]. The MCI reference was recorded with an accelerometer placed on the skin at the distal rectus femoris position using two-sided adhesive tapes. Krishnan et al. [10] improved the adaptive MCI cancellation technique with a 6th-order recursive least-squares (RLS) adaptive filter with the forgetting factor fixed at 0.98. The RLS adaptive filter provided two major advantages over the LMS adaptive filter. First, the convergence of the RLS algorithm was faster than that of the LMS algorithm. Second, the parameter (forgetting factor) of the RLS adaptive filter could be fixed, whereas the step size of the LMS filter had to be optimized with reference to input signal power, which varies with time spans. The results of the experiments of Krishnan et al. [10] indicated that MCI filtering was not an essential preprocessing step before feature extraction, and that the adaptive MCI cancellation step could make the results of VAG signal classification even worse. Based on such a conclusion, several subsequent studies related to VAG signal analysis [9, 16–18, 20] did not include the step of MCI reduction.

## References

1. Bak P, Tang C, Wiesenfeld K (1987) Self-organized criticality: an explanation of the  $1/f$  noise. *Phys Rev Lett* 59:381–384
2. Cai S, Wu Y, Xiang N, Zhong Z, He J, Shi L, Xu F (2012) Detrending knee joint vibration signals with a cascade moving average filter. In: *Proceedings of the 34th annual international conference of IEEE engineering in medicine and biology society*, San Diego, pp 4357–4360
3. Cai S, Yang S, Zheng F, Lu M, Wu Y, Krishnan S (2013) Knee joint vibration signal analysis with matching pursuit decomposition and dynamic weighted classifier fusion. *Comput Math Methods Med* 2013:Article ID 904267

4. Huang NE, Shen Z, Long SR, Wu MC, Shih HH, Zheng Q, Yen NC, Tung CC, Liu HH (1998) The empirical mode decomposition and the Hilbert spectrum for nonlinear and non-stationary time series analysis. *Proc R Soc Lond A* 454:903–995
5. Huang NE, Shen Z, Long SR (1999) A new view of nonlinear water waves: the Hilbert spectrum. *Annu Rev Fluid Mech* 31(1):417–457
6. Huang NE, Wu MLC, Long SR, Shen SSP, Qu W, Gloersen P, Fan KL (2003) A confidence limit for the empirical mode decomposition and Hilbert spectral analysis. *Proc R Soc Lond Ser A: Math, Phys Eng Sci* 459(2037):2317–2345
7. Kantelhardt JW, Koscielny-Bunde E, Rego HH, Havlin S, Bunde A (2001) Detecting long-range correlations with detrended fluctuation analysis. *Physica A* 295(3):441–454
8. Kim KS, Seo JH, Kang JU, Song CG (2009) An enhanced algorithm for knee joint sound classification using feature extraction based on time-frequency analysis. *Comput Methods Programs Biomed* 94(2):198–206
9. Krishnan S, Rangayyan RM (2000) Automatic de-noising of knee-joint vibration signals using adaptive time-frequency representations. *Med Biol Eng Comput* 38(8):2–8
10. Krishnan S, Rangayyan RM, Bell GD, Frank CB, Ladly KO (1997) Adaptive filtering, modelling, and classification of knee joint vibroarthrographic signals for non-invasive diagnosis of articular cartilage pathology. *Med Biol Eng Comput* 35(6):677–684
11. Lu M, Cai S, Zheng F, Yang S, Xiang N, Wu Y (2012) Adaptive noise removal of knee joint vibration signals using a signal power error minimization method. In: *Proceedings of the 7th international conference on computing and convergence technology*, Seoul, pp 1193–1196
12. Moussavi ZMK, Rangayyan RM, Bell GD, Frank CB, Ladly KO, Zhang YT (1996) Screening of vibroarthrographic signals via adaptive segmentation and linear prediction modeling. *IEEE Trans Biomed Eng* 43(1):15–23
13. Peng CK, Buldyrev SV, Goldberger AL, Havlin S, Sciortino F, Simons M, Stanley HE (1992) Long-range correlations in nucleotide sequences. *Nature* 356:168–170
14. Peng CK, Havlin S, Stanley HE, Goldberger AL (1995) Quantification of scaling exponents and crossover phenomena in nonstationary heartbeat time series. *Chaos* 5(1):82–87
15. Rangayyan RM (2002) *Biomedical signal analysis: a case-study approach*. IEEE/Wiley, New York
16. Rangayyan RM, Wu YF (2008) Screening of knee-joint vibroarthrographic signals using statistical parameters and radial basis functions. *Med Biol Eng Comput* 46(3):223–232
17. Rangayyan RM, Wu Y (2009) Analysis of vibroarthrographic signals with features related to signal variability and radial-basis functions. *Ann Biomed Eng* 37(1):156–163
18. Rangayyan RM, Wu Y (2010) Screening of knee-joint vibroarthrographic signals using probability density functions estimated with Parzen windows. *Biomed Signal Process Control* 5(1):53–58
19. Rangayyan RM, Krishnan S, Bell GD, Frank CB, Ladly KO (1997) Parametric representation and screening of knee joint vibroarthrographic signals. *IEEE Trans Biomed Eng* 44(11):1068–1074
20. Rangayyan RM, Oloumi F, Wu Y, Cai S (2013) Fractal analysis of knee-joint vibroarthrographic signals via power spectral analysis. *Biomed Signal Process Control* 8(1):26–29
21. Reddy NP, Rothschild BM, Mandal M, Gupta V, Suryanarayanan S (1995) Noninvasive acceleration measurements to characterize knee arthritis and chondromalacia. *Ann Biomed Eng* 23(1):78–84
22. Reddy NP, Rothschild BM, Verrall E, Joshi A (2001) Noninvasive measurement of acceleration at the knee joint in patients with rheumatoid arthritis and spondyloarthropathy of the knee. *Ann Biomed Eng* 29(12):1106–1111
23. Rilling G, Flandrin P (2008) One or two frequencies? The empirical mode decomposition answers. *IEEE Trans Signal Process* 56(1):85–95
24. Shen YP, Rangayyan RM, Bell GD, Frank CB, Zhang YT, Ladly KO (1995) Localization of knee joint cartilage pathology by multichannel vibroarthrography. *Med Eng Phys* 17(8):583–594

25. Tanaka N, Hoshiyama M (2012) Vibroarthrography in patients with knee arthropathy. *J Back Musculoskelet Rehabil* 25(2):117–122
26. Wu ZH, Huang NE (2004) A study of the characteristics of white noise using the empirical mode decomposition method. *Proce R Soc Lond Ser A: Math, Phys Eng Sci* 460(2046): 1597–1611
27. Wu ZH, Huang NE (2009) Ensemble empirical mode decomposition: a noise-assisted data analysis method. *Adv Adapt Data Anal* 1(1):1–41
28. Wu Y, Krishnan S (2011) Combining least-squares support vector machines for classification of biomedical signals: a case study with knee-joint vibroarthrographic signals. *J Exp Theor Artif Intell* 23(1):63–77
29. Wu Y, Rangayyan RM (2009) An unbiased linear adaptive filter with normalized coefficients for the removal of noise in electrocardiographic signals. *Int J Cogn Inform Nat Intell* 3(4): 73–90
30. Wu Y, Rangayyan RM (2011) Noise Cancellation in ECG Signals with an Unbiased Adaptive Filter. In: Wang YX (ed) *Transdisciplinary advancements in cognitive mechanisms and human information processing*. IGI Global, Hershey, pp 348–366
31. Wu Y, Rangayyan RM, Zhou Y, Ng SC (2009) Filtering electrocardiographic signals using an unbiased and normalized adaptive noise reduction system. *Med Eng Phy* 31(1):17–26
32. Wu Y, Krishnan S, Rangayyan RM (2010) Computer-aided diagnosis of knee-joint disorders via vibroarthrographic signal analysis: a review. *Crit Rev Biomed Eng* 38(2):201–224
33. Wu Y, Cai S, Xu F, Shi L, Krishnan S (2012) Chondromalacia patellae detection by analysis of intrinsic mode functions in knee joint vibration signals. In: *IFMBE proceedings of 2012 world congress on medical physics and biomedical engineering*, Beijing, vol 39, pp 493–496
34. Wu Y, Cai S, Yang S, Zheng F, Xiang N (2013b) Classification of knee joint vibration signals using bivariate feature distribution estimation and maximal posterior probability decision criterion. *Entropy* 15(4):1375–1387
35. Wu Y, Yang S, Zheng F, Cai S, Lu M, Wu M (2014) Removal of artifacts in knee joint vibroarthrographic signals using ensemble empirical mode decomposition and detrended fluctuation analysis. *Physiol Meas* 35(3):429–439
36. Zhang YT, Frank CB, Rangayyan RM, Bell GD, Ladly KO (1991) Step size optimization of nonstationary adaptive filtering for knee sound analysis. *Med Biol Eng Comput* 29(Suppl 2):836
37. Zhang YT, Frank CB, Rangayyan RM, Bell GD (1992) A comparative study of vibromyography and electromyography obtained simultaneously from active human quadriceps. *IEEE Trans Biomed Eng* 39(10):1045–1052
38. Zhang YT, Frank CB, Rangayyan RM, Bell GD (1992) Mathematical modeling and spectrum analysis of the physiological patello-femoral pulse train produced by slow knee movement. *IEEE Trans Biomed Eng* 39(9):971–979
39. Zhang YT, Rangayyan RM, Frank CB, Bell GD (1994) Adaptive cancellation of muscle contraction interference from knee joint vibration signals. *IEEE Trans Biomed Eng* 41(2):181–191

<http://www.springer.com/978-3-662-44283-8>

Knee Joint Vibroarthrographic Signal Processing and  
Analysis

Wu, Y.

2015, XIV, 81 p. 32 illus., 17 illus. in color., Softcover

ISBN: 978-3-662-44283-8